Globally Optimal Surface Segmentation Using Regional Properties of Segmented Objects

Xin Dou Xiaodong Wu
Andreas Wahle Milan Sonka
Department of Electrical and Computer Engineering
The University of Iowa, Iowa City, IA 52242, USA
{xdou,xwu3,awahle,sonka}@engineering.uiowa.edu

Abstract

Efficient segmentation of globally optimal surfaces in volumetric images is a central problem in many medical image analysis applications. Intra-class variance has been successfully utilized, for instance, in the Chan-Vese model especially for images without prominent edges. In this paper, we study the optimization problem of detecting a region (volume) between two coupled smooth surfaces by minimizing the intra-class variance using an efficient polynomial-time algorithm. Our algorithm is based on the shape probing technique in computational geometry and computes a sequence of minimum-cost closed sets in a derived parametric graph. The method has been validated on computer-synthetic volumetric images and in X-ray CT-scanned datasets of plexiglas tubes of known sizes. Its applicability to clinical data sets was demonstrated in human CT image data. The achieved results were highly accurate with mean signed surface positioning errors of the inner and outer walls of the tubes of $+0.013$*mm and* 0.012*mm, respectively, given a voxel size of* $0.39 \times 0.39 \times 0.6$*mm*^{3}*. Comparing with the original Chan-Vese method [8], our algorithm expressed higher robustness. With its polynomial-time efficiency, our algorithm is ready to be extended to higher-dimensional image segmentation. In addition, the developed technique is of its own interest. We expect that it can shed some light on solving other important optimization problems arising in computer vision. To the best of our knowledge, the shape probing technique is for the* first *time introduced into the field of computer vision.*

1. Introduction

Efficient segmentation of globally optimal surfaces in volumetric images is a central problem in many medical image analysis applications. While edges defined by image gradients are commonly used for segmentation, many object boundaries in medical image data may lack strong edges, e.g., when multiple adjacent objects with similar intensity profiles are present in an image. Image segmentation having the capability of handling weak edges is crucially important in medical image analysis. Intra-class variance has been successfully used in the novel Chan-Vese active contour model *without* using image gradient [8], which is based on a piecewise constant minimal variance criterion of the Mumford-Shah functional [20]. The following formula captures the intraclass variation, which is a very important part of the energy function used by Chan and Vese:

$$\mathcal{E}(\mathcal{S}) = \int_{inside(\mathcal{S})} |u_0(x,y,z) - c_1|^2 dxdydz + \int_{outside(\mathcal{S})} |u_0(x,y,z) - c_2|^2 dxdydz \quad (1)$$

where u_0 is the image, $\mathcal{S}$ is a variable boundary surface, and the constants c_1, c_2, depending on $\mathcal{S}$, are the averages of u_0 inside and outside $\mathcal{S}$, respectively. This energy function (intra-class variance) was proven capable of producing promising results [8]. However, Chan and Vese's method lacks the ability of finding the global optimality. Chan and Vese also considered two regularization terms in their energy function, which regularizing the length of the boundary and the area of the region. These regularization terms tend to smooth the boundary of the target object.

In this paper, we develop a novel algorithm that can find a globally optimal solution to segmentation by minimizing the *intra-class variance*. Our approach detects an optimal region between two coupled smooth surfaces in a volumetric image in a low-order polynomial time. Instead of adding the smoothness regularization term to the objective function as in the Chan-Vese model, we explicitly enforce the smoothness of the target surfaces with geometric constraints between neighboring voxels on the surfaces (see details in Section 2). The surface-coupled constraint

978-1-4244-2243-2/08/$25.00 ©2008 IEEE

may seem to highly limit the scope of this problem at first sight but in fact, the guarantee of global optimality and freedom to design a problem-specific cost function allow the method to be applied to a wide variety of medical image segmentation problems and it has been used in several medical practices [9, 24]. We show that the optimal solution can be obtained via the construction of the convex hull for a set of $O(n)$ unknown 2-D points using the shape probing technique [10, 12] in computational geometry, where n is the size of the input image. The probing oracles are implemented by computing a minimum s-t cut in a weighted directed graph. The intra-class variance can then be minimized by a sequence of calls to the minimum s-t cut algorithm. The shape probing technique was used for image segmentation [4, 23]. To the best of our knowledge, our method is the *first* algorithm for *globally* minimizing the intra-class variance to detect a region bounded by two coupled smooth surfaces in a volumetric image, and the shape probing technique is for the *first* time introduced into the field of computer vision. We believe that the developed technique is of its own interest and expect that it can shed some light on solving other important optimization problems arising in computer vision.

1.1. Previous Work

Several methods have been developed trying to globally optimize the Chan-Vese functional or related functionals. Chan *et al.* [7] developed global minimizers to the Rudin-Osher-Fatemi model from the research on denoising model and extended the idea to Mumford-Shah and Chan-Vese models. Based on their research, Bresson *et al.* [6] defined 3 new variational models (including the Chan-Vese functional) based on the unification of the classical snake/Geodesic Active Contour model, and developed global minimizers to their segmentation variational models and also fast minimization based on a dual formulation of the TV Norm. But in their approach, the mean intensities of the target object and the background are fixed in each iteration and updated occasionally to *approximate* the actual value of the average intensity. Li *et al.* [18] developed a graph searching based approach to approximate the Chan-Vese cost functional by estimating the mean intensity and their approach does not yield a globally optimal solution. An additional drawback is that their method can only detect the target object bounded by a single surface.

Boykov *et al*. [5] developed an approach to minimize the energy using minimum s-t cuts. A special class of edge-weighted directed graph $G_{st} = (V \cup \{s,t\}, E)$ was employed. The source s and the sink t are corresponding to object and background respectively. Edges enforce the constraints and create relationships between cuts and results. Grady [14] recently developed a method for computing discrete minimal surfaces using linear programming.

There are also other approaches that can globally optimize energy functions. Appleton *et al.* [1] used the shortest path approach to find the region minimizing the energy function, but only the region surrounded by a single contour can be found by this approach. They extended this research to 3D later [2], but it may suffer from numerical approximation and must be carefully designed to ensure the robustness and convergence. Ardon *et al.* [3] generalized globally minimal paths for curve segmentation in $2D$ to surface segmentation in $3D$. Their approach exploits the solution to the Eikonal equation and generates a function whose zero level set contains all the globally minimal paths between the constraining curves from two user-supplied curves, through a linear partial differential equation but not aiming at Chan-Vese functional.

Due to the imperfections of medical imaging techniques, insufficient image-derived information may be available for defining an object boundary or surface. This insufficiency can be remedied by using clues from the other mutually related boundaries or surfaces. Co-optimization of multiple coupled surfaces thus frequently yields superior results compared to the traditional single-surface detection approaches. Several methods for handling coupled surfaces have been proposed in recent years (e.g., [19][18]), they all demonstrate good performance in wide variety of medical image segmentation problems.

2. Problem Modelling

Let I be a given 3-D volumetric image of $n = X \times Y \times Z$ voxels, where X, Y, and Z denote the image sizes in $\mathbf{x}$, $\mathbf{y}$, and $\mathbf{z}$ directions, respectively. The intensity level of every voxel (x, y, z) ($1 \le x \le X, 1 \le y \le Y$, and $1 \le z \le Z$) is denoted by $I(x, y, z)$. We consider the desired region (target object) R that is bounded by two coupled terrain-like surfaces, S_l and S_u, and oriented as shown in Figure 1. Each of the bounding surfaces intersects with exactly one voxel of every *column* parallel to the $\mathbf{z}$-axis. We are looking for an *optimal region* by minimizing the intra-class variance among all feasible region that can be defined in the 3-D volumetric image I. Let μ_0 (resp., μ_1) be the average intensity of the desired region R (resp., the background $\overline{R} = I - R$), that is $\mu_0 = \frac{1}{|R|}\sum_{(x,y,z)\in R} I(x,y,z)$, and $\mu_1 = \frac{1}{|\overline{R}|}\sum_{(x,y,z)\in \overline{R}} I(x,y,z)$. The intra-class variance is

$$\mathcal{E}_{CV}(R) = \sum_{(x,y,z)\in R} (I(x,y,z) - \mu_0)^2 + \sum_{(x,y,z)\in \overline{R}} (I(x,y,z) - \mu_1)^2. \quad (2)$$

The feasibility of a region in I is constrained by two sets of application-specific parameters: (1) *surface smoothness parameters*, $\Delta_{\mathbf{x}}$ and $\Delta_{\mathbf{y}}$, and (2) *surface separation parameters*, δ^l and δ^u. The surface smoothness parameters guaran-

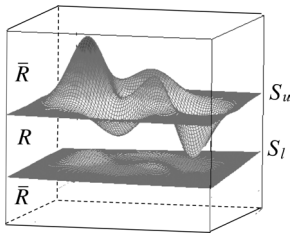

Figure 1. A region R enclosed by two coupled terrain-like surfaces S_l and S_u.

tee the continuity of the bounding surfaces of R. More precisely, if (x, y, z) and $(x+1, y, z')$ (resp., $(x, y+1, z')$) are two voxels on a feasible bounding surface, then $|z - z'| \leq \Delta_{\mathbf{x}}$ (resp., $\Delta_{\mathbf{y}}$). The surface separation parameters ensure that the two bounding surfaces, S_l and S_u, of the desired region R are at a certain distance range apart, that is, for every pair (x, y), $\delta^l \leq S_u(x, y) - S_l(x, y) \leq \delta^u$. Comparing to the regularizing terms used in Chan and Vese's method, our geometric constraints not only regulate the smoothness of the bounding surfaces, they also incorporate some shape information: the guarantee of monotonicity and topological constraints.

3. The Algorithm

Although minimizing the intra-class variance for general object shapes is computationally intractable, we are able to *optimally* detect the region bounded by two coupled terrain-like or cylindrical surfaces (a cylindrical transformation is used before performing our method) in low-order polynomial time using the techniques of parametric search [17], hand probing [10, 12] in computational geometry, and 3-D graph-searching [21, 18, 22].

Let $\mu = \frac{1}{n}\sum_{(x,y,z)\in I} I(x, y, z)$ be the average intensity of the entire image I. It is known that minimizing the intra-class variance $\mathcal{E}_{CV}(R)$ is equivalent to the maximization of the following objective function [16],

$$V(R) = |R|(\mu - \mu_0)^2 + |\overline{R}|(\mu - \mu_1)^2.$$

The equivalency of the two objective functions can be shown by comparing them,

$$\begin{aligned}
& \mathcal{E}_{CV}(R) \\
= & \sum_{(x,y,z)\in R} (I(x, y, z)^2 - 2\mu_0 I(x, y, z) + \mu_0^2) \\
& + \sum_{(x,y,z)\in \overline{R}} (I(x, y, z)^2 - 2\mu_1 I(x, y, z) + \mu_1^2) \\
= & \sum I(x, y, z)^2 - 2|R|\mu_0^2 + |R|\mu_0^2 - 2|\overline{R}|\mu_1^2 + |\overline{R}|\mu_1^2 \\
= & \sum I(x, y, z)^2 - |R|\mu_0^2 - |\overline{R}|\mu_1^2 \qquad (3)
\end{aligned}$$

$$\begin{aligned}
& -V(R) \\
= & -n\mu^2 + 2\mu(|R|\mu_0 + |\overline{R}|\mu_1) - |R|\mu_0^2 - |\overline{R}|\mu_1^2 \\
= & \left(\sum I(x, y, z)\right)^2 /n - |R|\mu_0^2 - |\overline{R}|\mu_1^2 \qquad (4)
\end{aligned}$$

Noticing that both $\sum I(x, y, z)^2$ and $(\sum I(x, y, z))^2/n$ are constants for a given image, the two objective functions differ by a constant, and thus minimizing $\mathcal{E}_{CV}(R)$ is equivalent to maximizing $V(R)$.

Note that the objective function $V(R)$ is invariant if we replace $I(x, y, z)$ by $\tilde{I}(x, y, z) = I(x, y, z) - \mu$ for every voxel (x, y, z) in I. Without loss of generality (WLOG), we thus assume that $\mu = 0$ and, accordingly,

$$\begin{aligned}
V(R) &= |R|\left(\frac{U(R)}{|R|}\right)^2 + |\overline{R}|\left(\frac{-U(R)}{|\overline{R}|}\right)^2 \\
&= \frac{n}{|R| \cdot |\overline{R}|}(U(R))^2, \qquad (5)
\end{aligned}$$

where $U(R) = \sum_{(x,y,z)\in R} I(x, y, z)$. Hence, WLOG, we can assume $U(R) \geq 0$, and thus minimizing $\mathcal{E}_{CV}(R)$ is equivalent to maximize

$$D(R) \equiv \frac{U(R)}{\sqrt{|R|(n - |R|)}} = \frac{\sum_{(x,y,z)\in R} I(x, y, z)}{\sqrt{|R|(n - |R|)}}. \qquad (6)$$

3.1. Overview of the Algorithm

Note that for each n_0 ($n_0 = 0, 1, \ldots, n$), if we can compute an optimal region $R^*(n_0)$ of size n_0 that maximizes the total sum of intensity of all pixels in the region (denoted by $U(R^*(n_0))$), then we solve the problem. Unfortunately, that is not an easy task at all. However, the view of the problem in such a way lays down a base for further exploiting the intrinsic geometric structure of the problem.

For each $n_0 = 0, 1, \ldots, n$, the pair $(n_0, U(R^*(n_0)))$ defines a point in the 2-D $|R| - U(R)$ coordinate plane, thus forming a set $\mathcal{P}$ of points. A key observation is that it may not be necessary to compute all points in $\mathcal{P}$. Here, a classical concept in computational geometry [11], called *convex hulls*, plays an important role. The convex hull $CH(\mathcal{P})$ of a set $\mathcal{P}$ is the unique convex polygon which contains $\mathcal{P}$ and all of whose vertices are points from $\mathcal{P}$.

We can show that the following lemma holds.

Lemma 1 *The point $(|R^*|, U(R^*))$ defined by an optimal region R^* in I (i.e., $D(R^*) = \max_R D(R)$), must be a vertex of the convex hull $CH(\mathcal{P})$.*

Proof. Let $\alpha^* = U(R^*)/\sqrt{|R^*|(n - |R^*|)}$. Consider the curve $\xi : y = \alpha^*\sqrt{x(n - x)}$ in the 2-D $|R|$-$U(R)$ plane. Since $U(R^*) = \alpha^*\sqrt{|R^*|(n - |R^*|)}$, the point

$(|R^*|, U(R^*))$ is on the curve ξ. Notice that $\alpha^* = \max_R\{U(R)/\sqrt{|R|(n-|R|)}\}$. Thus, for any region R bounded by two coupled smooth surfaces, we have $U(R) \leq \alpha^*\sqrt{|R|(n-|R|)}$, i.e., every point $(n_0, U(R(n_0)^*)) \in \mathcal{P}$ $(n_0 = 0, 1, \ldots, n)$ lies below or on the curve ξ (see Fig. 2). Furthermore, due to the concavity of $\sqrt{x(n-x)}$, all points in $\mathcal{P}$ lie below or on the tangent line l to ξ at the point $(|R^*|, U(R^*))$. Hence, $(|R^*|, U(R^*))$ is a vertex of the upper chain $UH(\mathcal{P})$ of the convex hull $CH(\mathcal{P})$ of $\mathcal{P}$. □

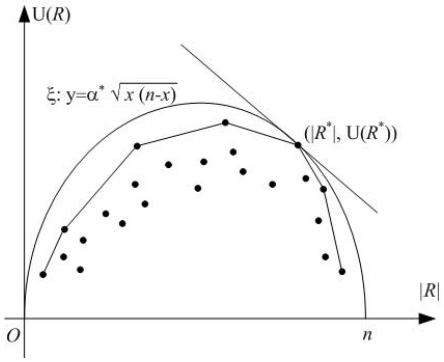

Figure 2. Illustrating the proof of Lemma 1

Thus, finding the optimum can be simplified to examining all the convex hull vertices. However, directly computing the hull vertices of $CH(\mathcal{P})$ appears to be quite involved. Inspired by the *shape probing* method[10, 12] which can be viewed as recognizing a convex polygon by "touching with lines", we use the following *probing oracle* to construct $CH(\mathcal{P})$ when the coordinates of the points in $\mathcal{P}$ are unknown.

Given a slope θ, report the tangent line with slope θ to $CH(\mathcal{P})$ and the tangent point.

Using this probing oracle, the convex hull $CH(\mathcal{P})$ can be constructed as follows. Start with slopes $+\infty$ and $-\infty$ to find the two endpoints of $\mathcal{P}$ (leftmost and rightmost points, which are always $(0, 0)$ and $(n, 0)$ in this algorithm). Note that the convex hull $\mathcal{P}$ actually is an upper convex chain. Now suppose that we have computed two vertices u and v on the hull and there is no vertex of $\mathcal{P}$ between u and v being computed so far. Let θ be the slope of the line through u and v. Then, perform a probing oracle with respect to θ (see Figure 3). Consequently, we either find a new vertex on $CH(\mathcal{P})$ between u and v or know that uv is an edge of $\mathcal{P}$.Thus, employing a probing oracle results in either a new vertex or a new edge of $\mathcal{P}$. Hence, the convex hull $CH(\mathcal{P})$ with k vertices can be computed with $O(k)$ probing oracles.

A major challenge is to implement this oracle for a given slope θ. The parametric approach [17] in computational geometry is utilized. For a given real-valued parameter θ, we define the parametric intensity sum of a region R as the sum of intensities of all pixels in R minus $\theta|R|$ (i.e., $U(R) - \theta|R|$), denoted by $U_\theta(R)$. We can show in Lemma 2 below, that the tangent point of the probing oracle is corresponding to the optimal feasible region with a maximized intensity sum in the parametric image I_θ ($I_\theta(x, y, z) = I(x, y, z) - \theta$ for every (x, y, z) tuple). This last step of the optimal-region-finding process can be modified and then solved using existing graph-based segmentation method.

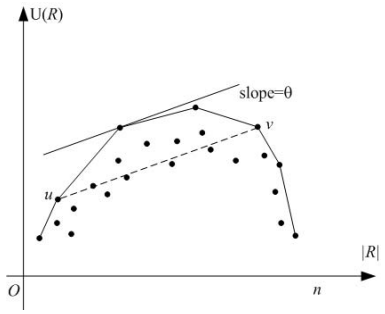

Figure 3. Illustrating the construction of a convex hull using the shape probing technique.

The algorithm can be summarized as follows.

MAIN(I)
1 $I_0 \leftarrow I - mean(I)$
2 SHAPEPROBE(I_0,0,0,n,0)

SHAPEPROBE(I,n_{left},U_{left},n_{right},U_{right})
1 $\theta \leftarrow (U_{right} - U_{left})/(n_{right} - n_{left})$
2 $I_\theta \leftarrow I - \theta$
3 Find the region $R^*(\theta)$ that maximizes $U_\theta(R(\theta))$ in I_θ.
4 **if** $|R^*(\theta)| \neq n_{right}$ **then do**
5 SHAPEPROBE(I,n_{left},U_{left},$|R^*(\theta)|$,$U(R^*(\theta))$)
6 SHAPEPROBE(I,$|R^*(\theta)|$,$U(R^*(\theta))$,n_{right},U_{right})

Input to the main program MAIN is the image I. Inputs to the subroutine SHAPEPROBE are the image I, the size coordinates and intensity-sum coordinates of two *known* vertices of the convex hull $CH(\mathcal{P})$ on the $|R|$-$U(R)$ plane. The subroutine SHAPEPROBE finds the hull vertices between the two input points. Line 1 calculates the slope θ. This parameter is used to find the tangent point by finding the optimal region in Line 3, in the parametric image calculated in Line 2. On the 4th Line, if a new hull vertex in between is found, the program recursively computes the hull vertices in the left and right intervals. The main program computes the upper chain of the convex hull $UH(\mathcal{P})$. Based on Lemma 1, we can examine every vertex of $CH(\mathcal{P})$ to find the optimum.

Theory and implementation details are given in the following sections. Section 3.2 introduces implementation details of the probing oracle and Section 3.3 gives a brief introduction to the calculation of the optimal parametric region.

3.2. Implementation of the Probing Oracle

Given a real-valued parameter θ, which is output by the shape probing procedure, we define the *total sum of the parametric intensity* of a desired region $R(\theta)$ as $U_\theta(R(\theta)) = \sum_{(x,y,z)\in R(\theta)} I_\theta(x,y,z)$. We show in this section that the probing oracle can be implemented via computing in I an optimal region $R^*(\theta)$ whose parametric intensity sum $U_\theta(R^*(\theta))$ is maximized. We call $R^*(\theta)$ an *optimal parametric region* associated with the parameter θ.

Lemma 2 *There exists a tangent line to $CH(\mathcal{P})$ at the point $(n_0, U(R^*(n_0)))$ with a slope θ if and only if $|R^*(\theta)| = n_0$ and $U(R^*(\theta)) = U(R^*(n_0))$.*

Proof. "⇒" Suppose that $l : y = \theta x + b$ is a tangent line to $CH(\mathcal{P}$ at the point $(j, U(R_j^*))$. This implies that $b = U(R_j^*) - j\theta = U(R_j^*) - |R_j^*|\theta$. Note that $UH(\mathcal{P})$ is the upper chain of the convex hull $CH(\mathcal{P})$. Thus for any $k \neq j$, the point $(k, k\theta + b)$ on l is on or above $UH(\mathcal{P})$. Alternatively, $k\theta + b \geq U(R_k^*)$, that is $U(R_j^*) - j\theta \geq U(R_k^*) - k\theta$ for any $k \neq j$ (see Fig. 4). Hence, the region R_j^* achieves $\max_k\{U(R_k^*) - k\theta\}$. Since R_j^* is an optimal coupled-surfaces-bounded region such that $|R_j^*| = j$ and $U_\theta(R_j^*) = \max_{R(\theta)} U(R(\theta))$, we know $U(R(\theta)) = U(R_j^*)$.

"⇐" The fact that $|R^*(\theta)| = j$ indicates that, for any coupled-surfaces-bounded region $R(\theta)$, if $|R(\theta)| \neq j$, then $U(R(\theta)) - |R(\theta)|\theta \leq U_\theta(R^*(\theta))$. Thus, for any $k \neq j$, $U(R_k^*) - k\theta \leq U_\theta(R^*(\theta))$. Based on the assumption that $U(R^*(\theta)) = U(R_j^*)$ and $|R^*(\theta)| = j$, we have $U(R_k^*) - k\theta \leq U(R_j^*) - j\theta$ for any $k \neq j$. Consider a line $l : y - \theta x = b$ with $b = U(R_j^*) - j\theta$. Obviously, the point $(j, U(R_j^*))$ is on the line l and the point $(k, U(R_k^*))$ is on or below the line l for any $k \neq j$ (see Fig. 4). Hence, line l is a tangent line to $CH(\mathcal{P})$ at the point $(j, U(R_j^*))$ with a slope θ. □

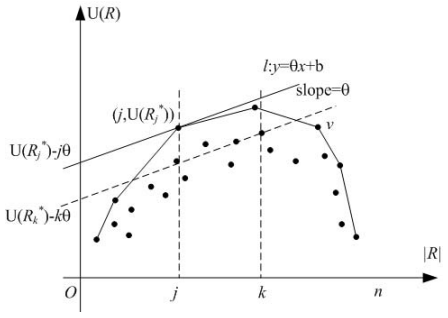

Figure 4. Illustrating the proof of Lemma 2

Consequently, for a given slope θ, we need to compute an optimal parametric region $R^*(\theta)$ bounded by two coupled terrain-like surfaces in I. If the size of $R^*(\theta)$ is n_0, based on Lemma 2, the line l: $y = \theta x + (U(R^*(\theta)) - n_0 \cdot \theta)$ is a tangent line to $CH(\mathcal{P})$ at the point $(n_0, U(R^*(\theta)))$ with slope θ. Let $R(n_0)^* = R^*(\theta)$. We thus recognize a hull vertex on $CH(\mathcal{P})$. Next, we develop an efficient algorithm for computing such an optimal parametric region $R^*(\theta)$ in I.

3.3. Computing an Optimal Parametric Region

Given a parameter θ, we reduce the problem of computing an optimal parametric region $R^*(\theta)$ in I to the problem of finding two coupled terrain-like 3-D surfaces on the transformed images while minimizing the total sum of the cost on both surfaces. This coupled terrain-like surfaces detection problem can be formulated as a surface segmentation problem proposed by Li *et al.* [18].

First, we perform the following transformations on the image I:

$$I'_\theta(x,y,z) = \begin{cases} 0 & \text{if } z = 0; \\ \sum_{0\leq z'<z}(I(x,y,z') - \theta) & \text{otherwise.} \end{cases} \tag{7}$$

and

$$I''_\theta(x,y,z) = \sum_{0\leq z'\leq z} -(I(x,y,z') - \theta). \tag{8}$$

Hence, for any feasible region $R(\theta)$ bounded by two coupled terrain-like surfaces, S_l and S_u, with S_u on top of S_l, we have

$$\sum_{(x,y,z)\in S_l} I'_\theta(x,y,z) + \sum_{(x,y,z)\in S_u} I''_\theta(x,y,z) = -U_\theta(R(\theta)). \tag{9}$$

Note that both bounding surfaces S_l and S_u satisfy the smoothness constraint and the surface separation constraint.

In this way, we convert the optimal parametric region problem to a surface segmentation problem. We next use Li *et al.*'s surface segmentation method to solve this problem [18].

The basic idea of Li *et al.*'s surface segmentation method is to transform the problem into computing a minimum s-t cut in a derived arc-weighted directed graph. Denote by $T(n', m')$ the time for finding a minimum s-t cut in an edge-weighted directed graph with $O(n')$ vertices and $O(m')$ edges. For example, using Goldberg and Tarjan's algorithm [13], $T(n', m') = O(m'n' \log \frac{n'^2}{m'})$.

Lemma 3 *For a given θ, an optimal parametric region $R^*(\theta)$ in I can be computed in $O(T(n, n))$ time.*

In summary, it suffices to compute the convex hull $CH(\mathcal{P})$ to detect in I an optimal region while minimizing the intra-class variance by Lemma 1. Based on Lemma 2, we can perform $O(n)$ probing Oracle steps to obtain all vertices on $CH(\mathcal{P})$. Each probing oracle can be implemented in $O(T(n, n))$ time by Lemma 3. Thus, the total running time of our algorithm for minimizing the intra-class variance is $O(nT(n, n))$. However, in our experimentation, the number of the probing oracle steps performed was much less than n.

4. Experiments

4.1. Data

To validate the correctness of the modelling techniques, we tested our method on a set of computer-generated phantoms containing differently textured regions or shapes, with sizes of $256 \times 256 \times 3$ voxels (Fig. 5).

To show the performance of our method in segmentation and to quantitively analyze the result, a physical phantom was imaged by multi-detector CT and analyzed using our method. The phantom contained six plexiglas tubes, numbered 1 through 6, with nominal inner diameters of 1.98, 3.25, 6.40, 6.50, 9.50 and 19.25mm, respectively. The corresponding outer diameters are 4.45, 6.30, 9.70, 12.60, 15.60 and 25.50mm, respectively. The phantom was scanned using Philips Mx8000 4-slice CT scanner with 3 different scan settings (low dose, regular dose, and high dose). Under each setting, the scans were taken at the 4 distinct angles of $0°$, $5°$, $30°$, and $90°$, rotated in the coronal plane, resulting in a total of 12 datasets for use in the validation. The regular dose scanning was intentionally repeated, yielding another 4 datasets used for initial calibration of the cost functions. In all cases, a resolution of $0.39 \times 0.39 \times 0.6mm^3$ was used, images consisted of 200-250 slices, 512×512 pixels each.

To demonstrate our method in quantitative analysis of human pulmonary CT images, the method was applied to concurrently segment the inner and outer wall surfaces of intrathoracic airways imaged by multi-detector CT. 20 sets of pulmonary CT images were used for the experiments.

4.2. The Cost Functions

Cost function design is very important in graph based segmentation. Since our method minimizes the intra-class variance, a cost function reflecting the homogeneity will be good for the experiments. So in most of the experiments we use the intensity or the linear transformation of the intensity as the cost of a voxel. For the texture related phantom images, we also add the orientation or curvature information to the cost function [8]. For the clinical data, our algorithm is run on the intensity image to get an estimated position of the bounding surfaces and then this estimated position information is combined with the voxel intensities to form the cost function.

4.3. Performance Indices

Surface detection accuracy was determined in physical phantoms in comparison with the independent standard. The mean signed surface positioning errors were computed and expressed in micrometers. Corresponding points were defined as pairs of points, the first point being from a computer detected border and the second point from the reference standard border that are closest to each other using the Euclidean distance metric. The local positioning errors were defined as the minimum distance from each computer-detected border pixel to reference standard.

5. Results

5.1. Computer Phantoms

Figure 5 presents segmentation examples obtained by our algorithm. The objects and background were differentiated by their different textures. The curvature and edge orientation in each slice were used (as descriptions of the patterns) for the cost functions. We also performed Chan and Vese's method on the same cost function and got similar results. But for Chan and Vese's method, the result is quite sensitive to the selection of coefficients of regularizing term. For some of the phantom images we tested (Figure 6), we failed to find appropriate coefficients to achieve a reasonable result (although it is possible that Chan and Vese's method could get the correct result with some coefficient combination), while our method worked smoothly.

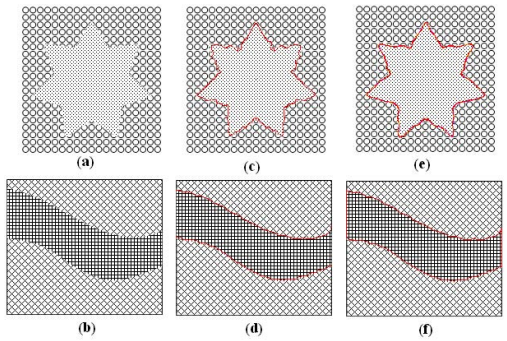

Figure 5. Computer phantoms and segmentation results.(a),(b) Original images. (c),(d) The segmentation results from our method, for (d), the inner boundary shrinks to the center of the image. (e),(f) The segmentation results from Chan and Vese's method.

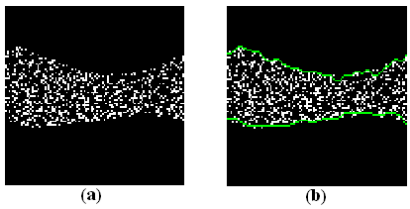

Figure 6. Computer phantoms and segmentation results.(a) Original images. (b) The segmentation results from our method.

5.2. Accuracy and Efficiency Assessment in Physical Phantom Tubes

The mean signed surface positioning errors of inner and outer walls are 0.013 ± 0.275mm and -0.012 ± 0.298mm, respectively, given a voxel size of $0.39 \times 0.39 \times 0.6\text{mm}^3$. The unsigned errors are 0.235 ± 0.150mm and 0.254 ± 0.160mm, for inner and outer walls respectively. In these experiments, less than 5% of the points on the $|R|$-$U(R)$ plane are on the convex hull $CH(\mathcal{P})$.

Using the original Chan and Vese's method and the same cost function as input to the method, we got signed errors of 0.311 ± 0.094mm and 0.097 ± 0.064mm, and unsigned errors of 0.411 ± 0.090mm and 0.359 ± 0.063mm. Comparing with Chan and Vese's method, our method has higher accuracy but lower consistency.

5.3. Results in Clinical Data

While inner airway wall surfaces are well visible in CT images, outer airway wall surfaces are very difficult to segment due to their blurred and discontinuous appearance. The results revealed a high accuracy and 3-D consistency (see Figure 7 and 8). Compared to the manual tracing-defined independent standard, our method yielded signed border positioning errors of 0.422 voxels and -0.127 voxels for inner and outer boundaries, respectively. The corresponding unsigned errors were 0.657 voxels and 0.572 voxels. We also tried to perform Chan and Vese's method on these data, but without the separation constraints, their method can not get reasonable result from our cost image.

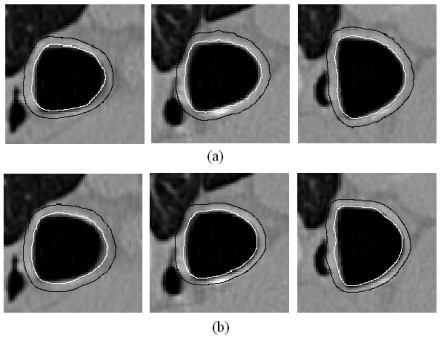

Figure 7. Comparison of computer-segmented and expert-traced inner and outer airway wall borders. (a) Expert-traced borders. (b) 3-D surface obtained using our method.

6. Discussion

6.1. Advantages and Limitations

The algorithm efficiently detects the globally optimal region in the entire region-of-interest (ROI), enabling highly accurate image segmentation that is a prerequisite of reliable quantitative image analyses. One obvious limitation is that only one region can be found by our method. Another apparent limitation is that it can only detect those surfaces that can be unfolded to be terrain-like, including cylindrical or tubular surfaces, and this unfolding process must be invertible. Closed surfaces and those target objects with complex shapes may require advanced unfolding techniques.

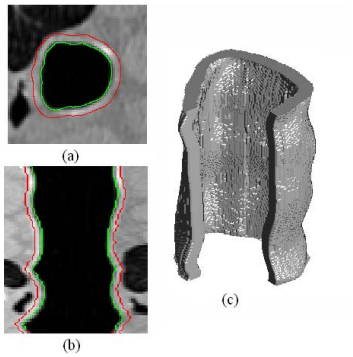

Figure 8. Segmented inner and outer walls of human pulmonary airways imaged with multi-detector CT. (a) The transverse, (b) sagittal cross-sections, and (c) 3-D view of an airway segment.

6.2. Possible Improvement

We noticed that in some clinical image segmentation cases, minimizing the intra-class variance alone may not guarantee good results. It is reasonable to use a combination of the intra-class variance term and an additional edge term in the objective function, that is,

$$\mathcal{E}(R) = \underbrace{\sum_{(x,y,z)\in S_l} c_l(x,y,z) + \sum_{(x,y,z)\in S_u} c_u(x,y,z)}_{\text{edge term}} + \underbrace{\sum_{(x,y,z)\in R} (I(x,y,z)-\mu_0)^2 + \sum_{(x,y,z)\in \overline{R}} (I(x,y,z)-\mu_1)^2}_{\text{intra-class variance term}}, \quad (10)$$

where S_l and S_u are the bounding surfaces of the region R and $c_l(x,y,z)$ (resp., $c_u(x,y,z)$) is the edge-based cost of voxel $I(x,y,z)$ for detecting the surface S_l (resp., S_u). However, it seems nontrivial to extend our algorithm for solving this generalized problem.

6.3. More Efficient Algorithm for Single Surface Case

In our method, the max-flow algorithm is performed for each parameter θ. This means the number of times that max-flow algorithm be executed depends on the number of vertices on the convex hull $CH(\mathcal{P})$. The execution of these max-flow algorithm dominates running time and so it is desirable to find a parametric max-flow algorithm to solve the

whole series of max-flow problems by performing the max-flow algorithm just once. By studying the characteristics of our graph used for optimal parametric region search, we found the following properties exist for the single surface case (i.e., the images is divided by a smooth terrain-like surface to two parts with one being the background and the other being the object) :

1) For edges from source to a vertex, the edge capacity is a nondecreasing function of θ;

2) For edges from a vertex to sink, the edge capacity is a nonincreasing function of θ;

3) For all other edges, the edge capacity is constant.

These satisfy the assumptions of parametric max-flow algorithm of Gusfield *et al.* [15] and we can accelerate our method by performing the max-flow algorithm once.

7. Conclusion

In this paper, we develop an algorithm to find globally optimal solution to segmentation by minimizing the intra-class variance. Our approach detects an optimal region bounded by two coupled smooth surfaces in a volumetric image in a low-order polynomial time.

We employed the techniques of parametric search, shape probing in computational geometry, and 3-D graph-search. The method has been validated by computer-synthetic volumetric images and medical datasets.

References

[1] B. Appleton and H. Talbot. Globally optimal geodesic active contours. *Journal of Mathematical Imaging and Vision*, 23:67–86, 2005.

[2] B. Appleton and H. Talbot. Globally minimal surfaces by continuous maximal flows. *IEEE Transactions on Pattern Analysis and Machine Intelligence*, 28(1):106–118, 2006.

[3] R. Ardon, L. Cohen, and A. Yezzi. A new implicit method for surface segmentation by minimal paths: Applications in 3d medical images. *EMMCVPR05*, pages 520–535, 2006.

[4] T. Asano, D. Chen, N. Katoh, and T. Tokuyama. Efficient algorithms for optimization-based image segmentation. *International Journal of Computational Geometry & Applications*, 11(2):145–166, 2001.

[5] Y. Boykov and G. Funka-Lea. Graph cuts and efficient n-d image segmentation. *International Journal of Computer Vision*, 70(2):109–131, 2006.

[6] X. Bresson, S. Esedoglu, P. Vandergheynst, J. Thiran, and S. Osher. Fast global minimization of the active contour/snake model. *Submitted to Journal of Mathematical Imaging and Vision*, 2005.

[7] T. Chan, S. Esedoglu, and M. Nikolova. Algorithms for finding global minimizers of image segmentation and denoising models. *UCLA CAM Report 04-54*, 2004.

[8] T. Chan and L. Vese. An active contour model without edges. *IEEE Transactions on Image Processing*, 10(2):266–277, 2001.

[9] M. Chung, W. Worsley, T. Paus, S. Robbins, J. Taylor, J. Giedd, J. Rapoport, and A. Evans. Detecting gray matter maturation via tensor-based surface morphometry. In *9th Annual Meeting of the Organization for Human Brain Mapping*, 1999.

[10] R. Cole and C. Yap. Shape from probing. *Journal of Algorithms*, 8(1):19–38, 1987.

[11] M. de Berg, M. van Kreveld, M. Overmars, and O. Schwarzkopf. *Computational Geometry: Algorithms and Applications, 2nd Edition*. Springer-Verlag Berlin Heidelberg New York, 2000.

[12] D. Dobkin, H. Edelsbrunner, and C. Yap. Probing convex polytopes. *Proceeding of 18th Annual ACM Symposium on Theory of Computting*, pages 387–392, 1986.

[13] A. Goldberg and R. Tarjan. A new approach to the maximum-flow problem. *Journal of the ACM*, 35:921–940, 1988.

[14] L. Grady. Computing exact discrete minimal surfaces: Extending and solving the shortest path problem in 3d with application to segmentation. *2006 IEEE Computer Society Conference on Computer Vision and Pattern Recognition (CVPR'06)*, 1:69–78, 2006.

[15] D. Gusfield and E. Tados. A faster parametric minimum-cut algorithm. *Algorithmica*, 11(3):278–290, 1994.

[16] D. Hand. *Discrimination and Clasification*. John Wiley & Sons, 1981.

[17] N. Katoh and T. Ibaraki. A parametric characterization and an ϵ-approximation scheme for the minimization of a quasi-concave program. *Discrete Applied Mathematics*, 17:39–66, 1987.

[18] K. Li, X. Wu, D. Chen, and M. Sonka. Globally optimal segmentation of interacting surfaces with geometric constraints. *2004 IEEE Computer Society Conference on Computer Vision and Pattern Recognition (CVPR'04)*, 1:394–399, 2004.

[19] D. MacDonald, N. Kabani, D. Avis, and A. Evans. Automated 3-d extraction of inner and outer surfaces of cerebral cortex from mri. *NeuroImage*, 12(3):340C356, 2000.

[20] D. Mumford and J. Shah. Optimal approximation by piecewise smooth functions and associated variational problems. *Commun. Pure Appl. Math*, 42:577–685, 1989.

[21] X. Wu and D. Chen. Optimal net surface problems with applications. *29th International Colloquium in Automata, Languages and Programming(ICALP '02)*, pages 1029–1042, 2002.

[22] X. Wu, D. Chen, K. Li, and M. Sonka. The layered net surface problems in discrete geometry an medical image segmentation. *Proceeding of 16th International Symposium. Algorithms and Computation*, 2005.

[23] X.Wu. Efficient algorithms for the optimal-ratio region detection problems in discrete geometry with applications. *Accepted to the 17th International Symposium on Algorithms and Computation (ISAAC'06)*, Kolkata, India, 18-20, Dec.2006.

[24] X. Zeng, L. Staib, R. Schultz, and J. Duncan. Segmentation and measurement of the cortex from 3d mr images using coupled surfaces propagation. *IEEE Transactions on Medical Imaging*, 18(10):100–111, 1999.